THE ARCHIVE OF MECHANICAL ENGINEERING

Vol. L 2003 Number 3

Key words: *transonic flows, airfoil loading*

*Z. NOSAL**), *W. C. SELEROWICZ***)

THE EFFECT OF AIR HUMIDITY ON BUFFET PHENOMENON

The effect of air humidity on transonic flow around an NACA0012 airfoil at flow conditions, characteristic for buffet phenomenon, was investigated experimentally. Airfoil angles of attack in the range from 6° up to 10° were used, whereas values of initial relative air humidity were kept constant at four values 12%, 40%, 60% and 80%. Reconstructed time depending airfoil pressure distributions, time histories of normal aerodynamic force coefficient C_n as well values of C_n pulsation are shown on the basis of surface pressure measurements at various humidity levels. The influence of the air humidity on the buffet origin is presented.

1. Introduction

The buffet phenomenon appears at high angle-of-attack flight conditions, frequently encountered during aircraft combat maneuvers, landing and take-off phases of a flight, cruise operation in severe gust conditions [1], [2]. Then, the large regions of flow separation exist over the wing and fuselage. The separated flow field, characterized by big unsteadiness and strong vortical flow structure, can interact with various component of the aircraft such as canards, fin and tailplane, flaps, rear fuselage. The aerodynamic excitation caused by separated flows limit the maneuvering capability of an aircraft and affect its structural safety. An important problem, frequently described in many recent papers [3], [4], is the buffeting of tail immersed in separated wake behind a wing – fuselage interface and leading – edge extensions.

*) *Warsaw University of Technology, Institute of Aeronautics and Applied Mechanics, ul. Nowowiejska 24, 00-665 Warsaw, Poland; E-mail: znos@meil.pw.edu.pl*

**) *Warsaw University of Technology, Institute of Aeronautics and Applied Mechanics, ul. Nowowiejska 24, 00-665 Warsaw, Poland; E-mail: seler@meil.pw.edu.pl*

The solution of the buffet problems may be adaptive wing and flow control technology (slats at the leading-edge, leading-edge/trailing-edge flaps system, leading-edge blowing, boundary layer suction) [5], [6], [7], which adjust the flow development to the prevailing flight condition changing considerably during an aircraft mission. By this means, the onset of flow separation is reduced or delayed and then the buffet onset boundaries improve.

The buffet phenomenon is closely associated to airfoil transonic flow. In such conditions, the unsteady aerodynamic loads are far more sever than those at low subsonic speed. It is a result of typical airfoil transonic flowfield unsteadiness with locally supersonic region terminated by a shock wave whose strength grow up during motion downstream. The unsteady pressure fluctuations are driven by the interaction of a shock wave with a boundary layer [8], [9], [10]. This effects initially thicken the boundary layer, next develop shock induced separation bubble and finally cause rear separation with periodic shock motion on airfoils. The aerodynamic excitations associated with separated flows are normally random in character and cover a wide frequency range, but sometime are coupled with some form of aerodynamic resonance [1], [5].

The air humidity may considerably affect the transonic flow because of many possible gasodynamic phenomena. The humid air flow may change the phase by vapour condensation in the fast expansions regions typical for transonic flow around airfoil. It follows the heat release, droplets formation, multi-phase mixture flow. This effects explain the sensitive reaction of transonic flows over airfoils caused by the shock shifting and oscillation, changing the pressure distribution and resulting in aerodynamic characteristics of the flow. This phenomenon confirms the well know uncommon images of the modern combat aircraft in transonic flight with condensation and evaporation of the water vapour regions where the flow has expanded on wings.

The experimental investigations of the influence of the wet air on transonic airfoil flow was reported in papers [11], [12], [13], and gained the interest for buffet study in this conditions. The humidity modify the principal transonic phenomena such as shock wave boundary layer interaction and flow separation.

The experimental simulations of these unsteady flows are under the limitations inherent in wind-tunnel tests with separated flow on the airfoil, the scale effects may be significant because of rather small Reynolds numbers [14].

2. Experimental set-up

All experiments described in present paper were done in transonic wind tunnel of short time operation which is schematically shown in Fig. 1. The air is sucked from an elastic reservoir 1 having a volume of approximately 50 m^3 into a vacuum tank 2 of 150 m^3 through a tunnel test section of 100 mm width, 440 mm height and 1000 mm length. The duration of the tunnel operation depends on the cut-off valve 3 settings and is 1s of typical order. This time is sufficient to achieve a steady conditions in a test section as well to store all measured data. The velocity of the tunnel main flow is regulated by means of the control valve 4.

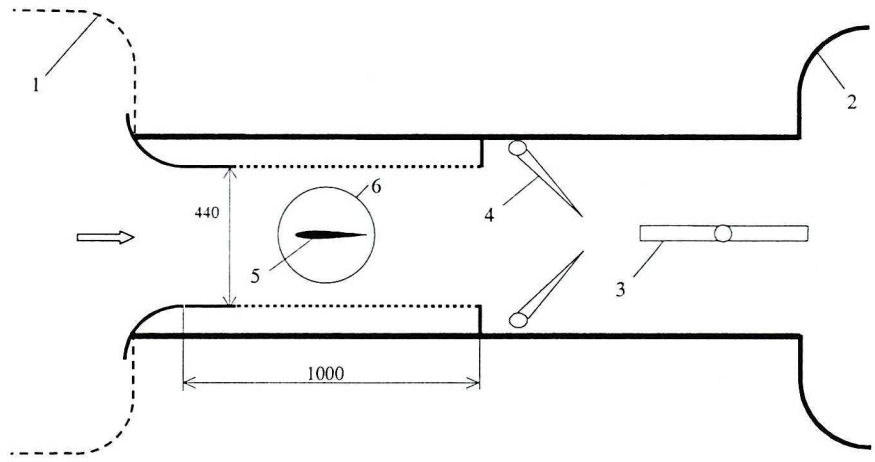

Fig. 1. Scheme of the transonic wind tunnel test section arrangement: 1 – elastic reservoir, 2 – vacuum tank, 3 – cut-off valve, 4 – control valve, 5 – NACA 0012 airfoil, 6 – glass window used in flow visualisation

The use of the elastic reservoir was necessary for precise preparation of the inlet air conditions. The air temperature in the reservoir was kept constant at 22°C during all experiments, whereas the relative air humidity was changed in four steps: 12% (dry inlet air), 40%, 60% and 80% (humid air). During the tunnel operation, the air temperature decreased from 22°C in the reservoir (stagnation conditions) up to −4°C in the tunnel test section. At the same time, the air relative humidity increased from its stagnation value up to 40% in the first case and up to 100% in the second one. In the last two cases (initial humidity level 60% and 80%), overcooling vapour conditions were reached after expansion to the test section conditions. However, the condensation of the main stream was never observed in the tunnel test section. This phenomenon was registered only on the airfoil upper surface close to the airfoil nose.

All reported experiments were performed with a symmetric NACA0012 airfoil of 120 mm chord length, located in the central part of the tunnel test section. It was specially prepared for steady as well for unsteady pressure measurements. In the first case, 22 holes of 0.33 mm diameter bored on the airfoil surface were connected with a pressure scanner by means of elastic mini-pipes. For measurements of pressure fluctuations, a set of 13 miniature Kulite piezoresistive transducers was assembled inside the model, as shown in Fig. 2. An additional pressure transducer was mounted near the airfoil trailing edge on the tunnel side wall.

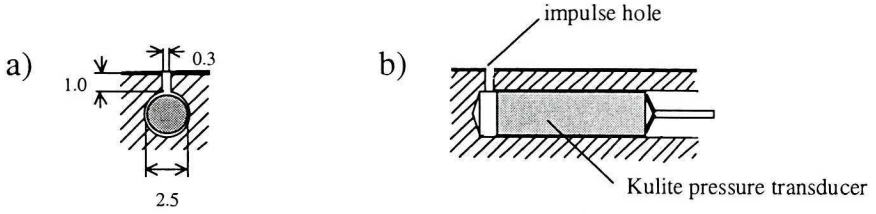

Fig. 2. Details of the Kulite pressure transducer installation: a) front view, b) main view

In all experiments, the free-stream Mach number was kept constant at $M = 0.7$. The Reynolds number based on the free-stream tunnel velocity and chord length was 2×10^6. The airfoil angle of attack was changed between $\alpha = 6°$ and $\alpha = 10°$ with a step of 0.5°.

3. Results

3.1. Average pressure distributions

Figures 3a, 3b and 3c show average pressure distributions obtained on the upper and bottom airfoil surfaces at three angles of attack $\alpha = 6°$, $\alpha = 8°$ and $\alpha = 10°$. On each figure, curves representing four values of relative air humidity are presented.

As it can be seen in Fig. 3a, at lowest angle of attack, under consideration, the influence of the humidity level is inessential on the bottom surface. Pressure distributions measured on the upper airfoil surface show two typical cases, the first one (humidity 12% and 40%) corresponds to transonic airfoil flow shock induced boundary layer separation. The second one (humidity 60% and 80%) is the flow with shock-boundary layer interaction without separation. The humidity causes then qualitative change of the airfoil flow which is very important for the buffet phenomenon. The shock wave intensity

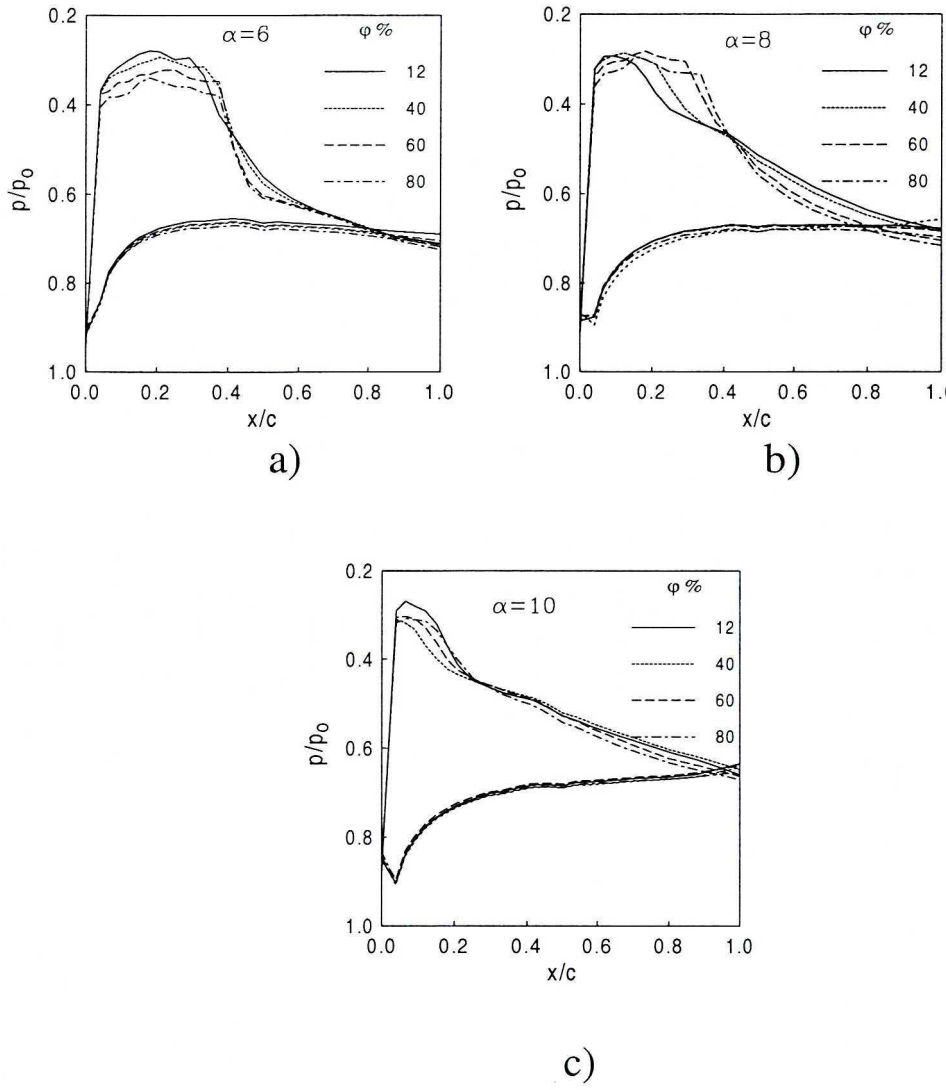

Fig. 3. Average pressure distributions on the airfoil upper and bottom surface at Mach number $M_\infty = 0.7$. The angle of attack values are: a) $\alpha = 6°$, b) $\alpha = 8°$, c) $\alpha = 10°$.

decreases with the increase of air humidity. The subsequent behaviour of the flow in a supersonic flow region (a first half of the airfoil) is a strong function of the humidity and creates a series of compression waves with complicated flow structure. The minimum pressure ratio obtained at humidity $\varphi = 12\%$ was about 0.28, whereas at $\varphi = 80\%$ it was at least 0.34. It is also interesting that the pressure increase observed at $x/c \approx 0.4$, which denotes the existence of a shock on the upper surface, is stronger for air humidity $\varphi = 60\%$ and $\varphi = 80\%$

than that for $\varphi = 40\%$ and especially for $\varphi = 12\%$. To explain such a situation, a flow visualisation using Schlieren method with long exposure time was performed. The results are presented in Fig. 4 ($\alpha = 6°$) and Fig. 5 ($\alpha = 8°$). From the picture in Fig. 4a (humidity level 12%) one can draw a conclusion that the shock on the upper surface must not be fully stable, because it is not sharp. At humidity $\varphi = 40\%$, the shock is visibly sharper. The best pictures of the shock can be obtained from Fig. 4c and 4d (humidity levels 60% and 80%). In both cases, the shock is preceded by a set of condensation waves (the main stream is now overcooled, what leads to vapour condensation in the regions of low pressure).

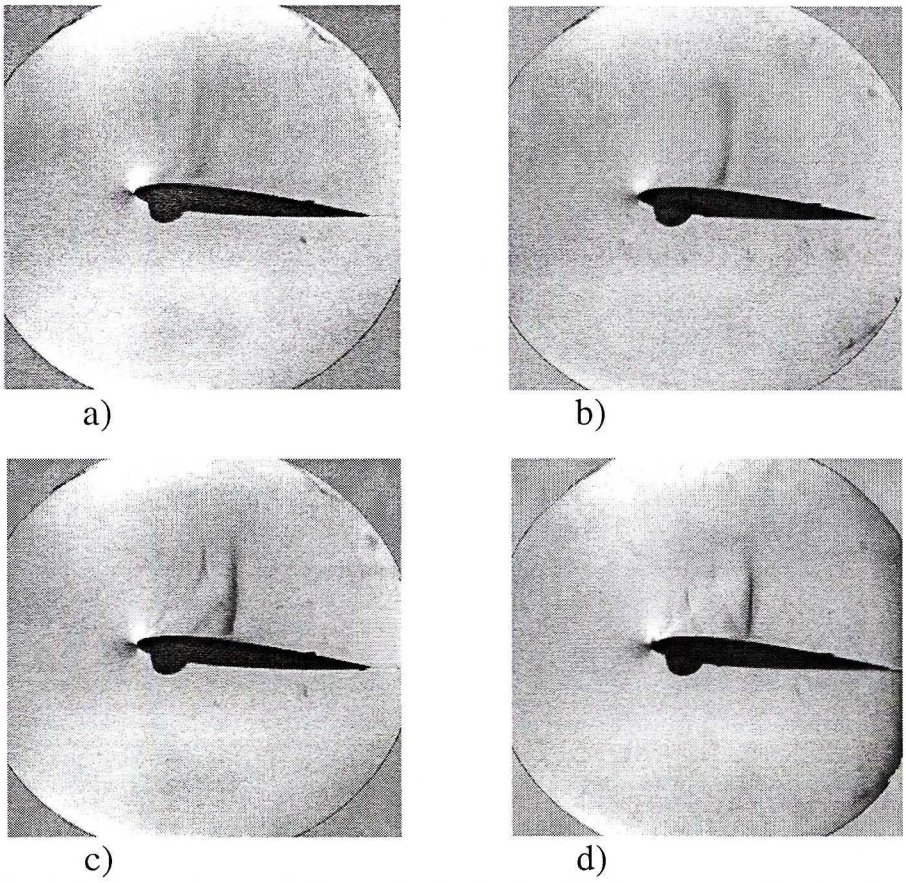

Fig. 4. Airfoil flow visualisation (Schlieren method) using prolonged exposure. $M_\infty = 0.7$, $\alpha = 6°$. Values of initial relative air humidity φ are: a) 12%, b) 40%, c) 60%, d) 80%.

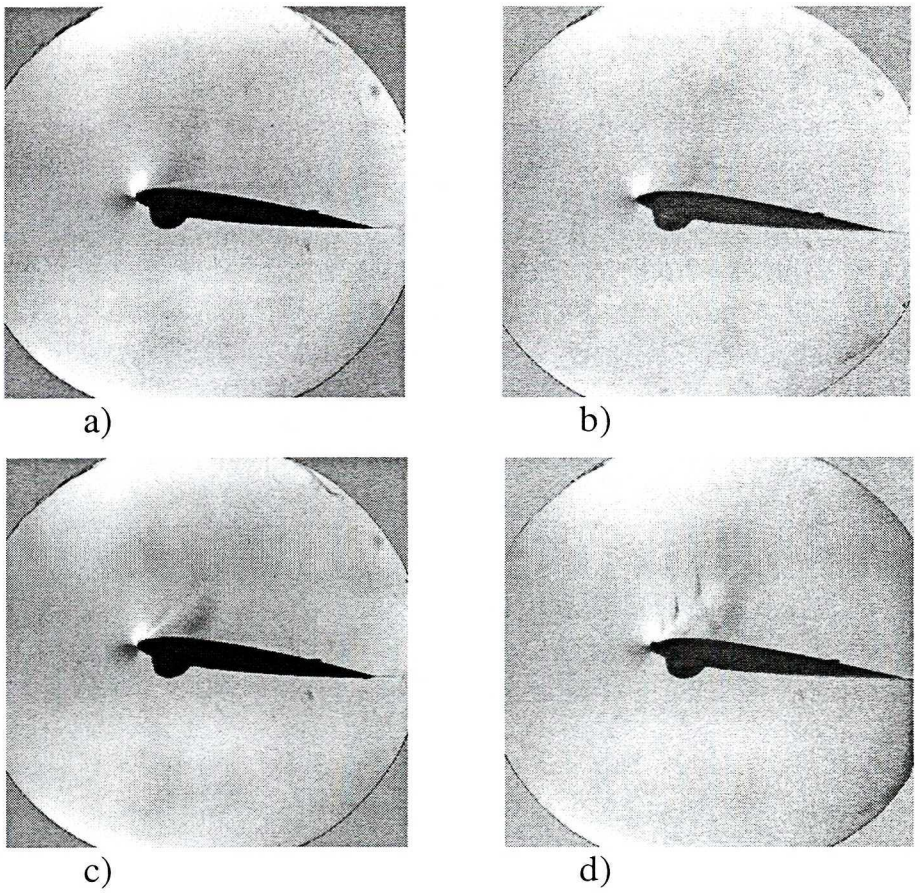

Fig. 5. Airfoil flow visualisation (Schlieren method) using prolonged exposure. $M_\infty = 0.7$, $\alpha = 8°$. Values of initial relative air humidity φ are: a) 12%, b) 40%, c) 60%, d) 80%.

Pressure distributions obtained at $\alpha = 8°$ (Fig. 3b) show, contrary to $\alpha = 6°$, distinct differences on the upper surface, whereas on the bottom one, likewise at $\alpha = 6°$ (Fig. 3a) and $\alpha = 10°$ (Fig. 3c) distributions are nearly identical. The largest changes can be observed for humidity level $\varphi = 12\%$, because the pressure distributions do not remind the shape characteristic for a flow with shock. On the other hand, pressure traces representing higher humidity levels ($\varphi = 60\%$ and $\varphi = 80\%$) are nearly the same as the curve for $\varphi = 12\%$ at $\alpha = 6°$. Additional observations can be made on the basis of Fig. 5. In picture a) ($\varphi = 12\%$) no more shock can be noticed, because there exists a strong oscillation in these flow conditions.

To confirm this supposition, instantaneous pressure traces obtained from shock oscillation region are shown in Fig. 6 for the considered airfoil angle of attack. Pressure signals at $\alpha = 8°$, taken at $x/c = 0.29$, show strong pressure

variations for $\varphi = 12\%$ (due to the shock oscillation), much smaller for $\varphi = 40\%$ and almost insignificant for $\varphi = 60\%$ and $\varphi = 80\%$. In the two latter cases, weak shock waves closing the condensation regions can be still distinguished.

Pressure distributions obtained at high angle of attack ($\alpha = 10°$) shown in Fig. 3c are characterised again by smaller differences, with an exemption of the curve for $\varphi = 12\%$. The regions of pressure minimum on the airfoil upper (suction) surface enlarges with the increase of the humidity level from $\varphi = 40\%$ up to $\varphi = 80\%$. From pressure traces shown in Fig. 6c one can deduce, that the shock oscillation is now higher for $\varphi = 40\%$ than for $\varphi = 80\%$. In contrast, the pressure trace for $\varphi = 12\%$ shows fragmentary disappearance of the shock oscillation. This explains the other shape of pressure distribution. In this case, the pictures from flow visualisation are not presented. Due to the high level of flow oscillation, the shock identification is impossible irrespective of humidity level of air.

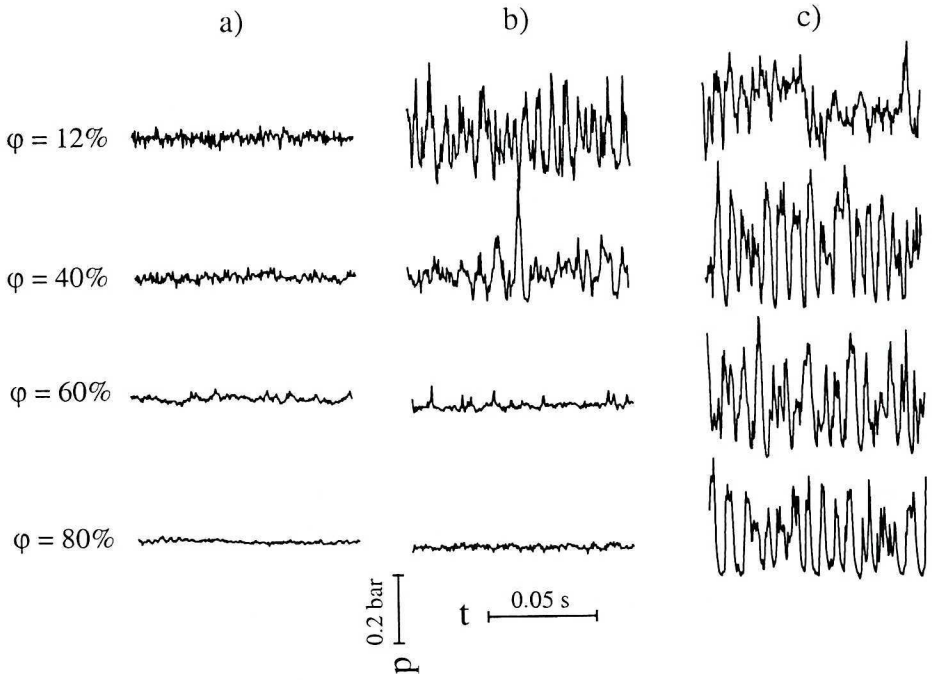

Fig. 6. Pressure signals obtained in characteristic places on the airfoil upper surface at $M_\infty = 0.7$. Values of angle of attack α and x/c location are: a) $\alpha = 6°$, x/c = 0.38, b) $\alpha = 8°$, x/c = 0.29, c) $\alpha = 10°$, x/c = 0.21. Time and pressure scales are the same for all traces.

3.2 Surface pressure pulsations

RMS values of pressure pulsations calculated from pressure signals measured on the upper airfoil surface and plotted versus chord length are

shown in Fig. 7 for all humidity levels under consideration. Distributions shown in Fig. 7a ($\alpha = 6°$) are characteristic for a pattern with stationary shock. For dry air, it is accompanied by flow separation, whereas for strong humid air (last two cases), the flow behind shock is attached (pressure pulsations decrease up to x/c = 0.85). One can draw a general conclusion that the increase of the humidity level leads to flow stabilisation associated with decreasing of pressure pulsations.

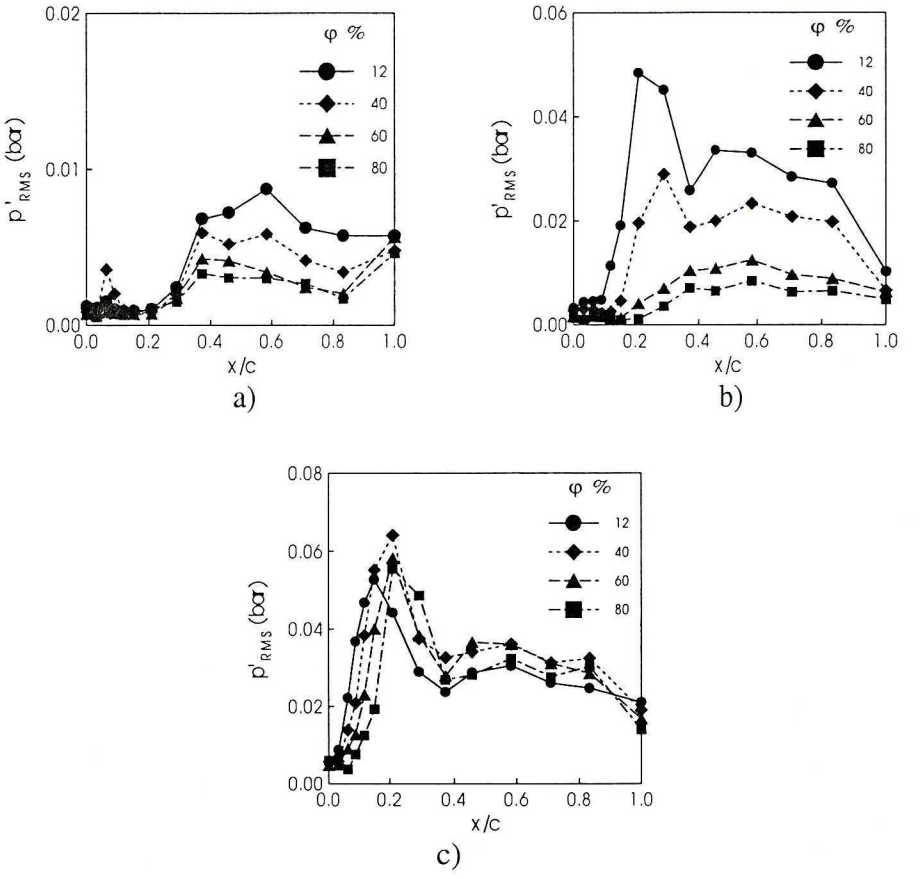

Fig. 7. RMS values of pressure pulsation (on the upper surface only) for several humidity levels versus chord length at $M_\infty = 0.7$. Values of angle of attack are: a) $\alpha = 6°$, b) $\alpha = 8°$, c) $\alpha = 10°$.

In contrast to Fig. 7a, values of pressure pulsations shown in Fig. 7b ($\alpha = 8°$) are of about 5 times higher. Distributions obtained for dry and semi-humid air ($\varphi = 12\%$ and 40%) denote a flow with oscillating shock (first peak at x/c = 0.2) and subsequent flow separation (renewed RMS increase at x/c = 0.6). At this airfoil angle of attack, a flow pattern with stationary shock

can be assumed for humidity level $\varphi = 60\%$ and 80% only. In both cases, subsequent flow attachment can be well established.

At highest angle of attack under consideration ($\alpha = 10°$), all pressure pulsations have similar shape (see Fig. 7c). Curves for $\varphi = 40\%$, 60% and 80% have a maximum exactly at $x/c = 0.2$ like in Fig. 7b whereas values for $\varphi = 12\%$ are a little lower and the first peak occurs just at $x/c = 0.15$. This permits a conclusion that in the last case a flow pattern characterised by fully separation from edge of attack is achieved. RMS values of pressure pulsations are maximal at this angle of attack.

3.3. Instantaneous airfoil loading

Instantaneous pressure coefficient distribution was calculated from pressure signals recorded from Kulite transducers at 14 points on the airfoil upper surface. The value of C_p was determined from the formula

$$C_p = \frac{\frac{p}{p_\infty} - 1}{\frac{1}{2} k M_\infty^2}$$

where: C_p – time depending pressure coefficient,
p – momentary pressure on airfoil upper surface,
p_∞ – free-stream pressure,
M_∞ – free-stream Mach number,
k – isentropic exponent.

Momentary C_p distributions versus the nondimentional chord length x/c are presented for all humidity levels under consideration in Fig. 8 for airfoil angle of attack $\alpha = 6°$, in Fig. 9 for $\alpha = 8°$ and in Fig. 10 for $\alpha = 10°$. In all plots, the time interval between two successive C_p distributions is $\Delta t = 0.4$ms. Due to the inessential influence of the humidity level on the pressure signals on the bottom airfoil surface, only distributions on the upper surface are presented.

According to plots shown in Fig. 4 ($\alpha = 6°$), flow with steady shock on the upper surface can be assumed irrespective of air humidity level. At $\varphi = 12\%$ (Fig. 8a) only very small differences in C_p distributions can be noticed in the rear part of the airfoil ($x/c > 0.7$). This confirms that at $\alpha = 6°$ the buffet phenomenon does not exist on the airfoil.

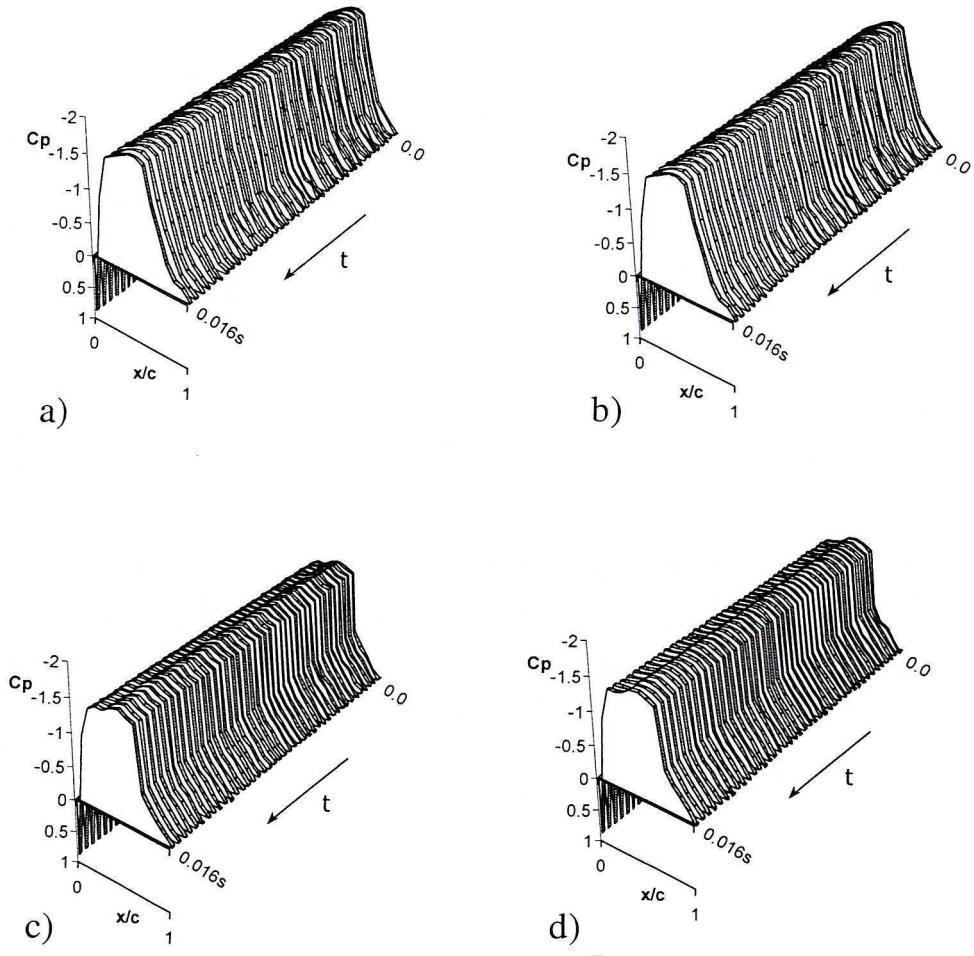

Fig. 8. Momentary pressure distribution on the airfoil upper surface. Free-stream Mach number $M_\infty = 0.7$. Airfoil angle of attack $\alpha = 6°$. Values of initial relative air humidity φ are: a) 12%, b) 40%, c) 60%, d) 80%.

The situation rapidly changes when the angle of attack $\alpha = 8°$ is considered (Fig. 9). Plot in Fig. 9a ($\varphi = 12\%$) shows considerable differences in successive C_p distributions. Some of them have a shape characteristic for a flow with shock, whereas the others exhibit a shape characteristic for a fully separated flow.

With increasing air humidity (Fig. 9b $\varphi = 40\%$), irregularities in C_p distributions are still well visible, although they are not so distinctive as for $\varphi = 12\%$. At humidity levels $\varphi = 60\%$ and $\varphi = 80\%$ (Fig. 9c and 9d respectively) a steady flow can be deduced from the plots.

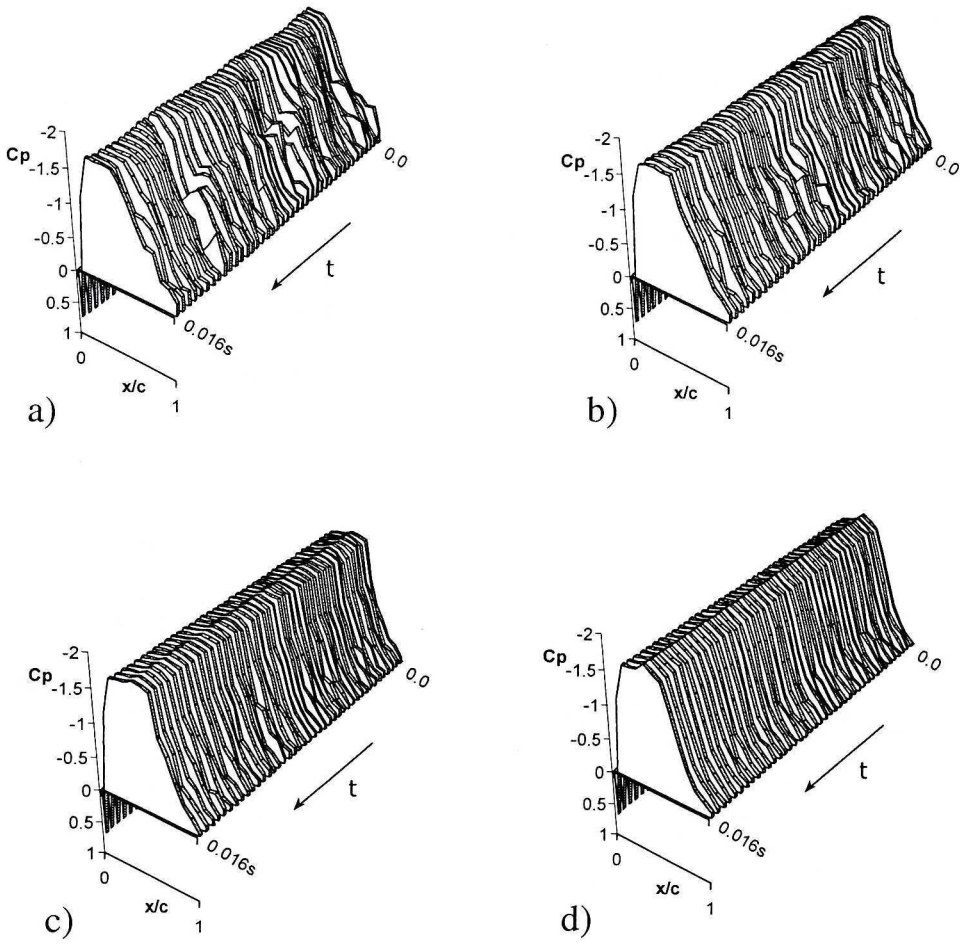

Fig. 9. Momentary pressure distribution on the airfoil upper surface. Free-stream Mach number $M_\infty = 0.7$. Airfoil angle of attack $\alpha = 8°$. Values of initial relative air humidity φ are: a) 12%, b) 40%, c) 60%, d) 80%.

At the highest angle of attack under consideration, a fully unsteady flow, irrespective of the humidity level of air, can be confirmed by C_p distributions (Fig. 10, $\alpha = 10\%$). It is to note that according to Fig. 10a ($\varphi = 12\%$) one can preferably assume a fully separated flow whereas other plots rather indicate a flow with oscillating shock.

Instantaneous C_p distributions, shown in Figures 8, 9 and 10 facilitated the calculation of time depending aerodynamic normal force coefficient (the suction surface component only) from the formula

$$C_n = -\int_0^1 C_p \, d\left(\frac{x}{c}\right)$$

where: C_n (t) – time depending aerodynamic force coefficient,
C_p (t) – momentary pressure coefficient at the upper airfoil surface,
x/c – non-dimensional cord length.

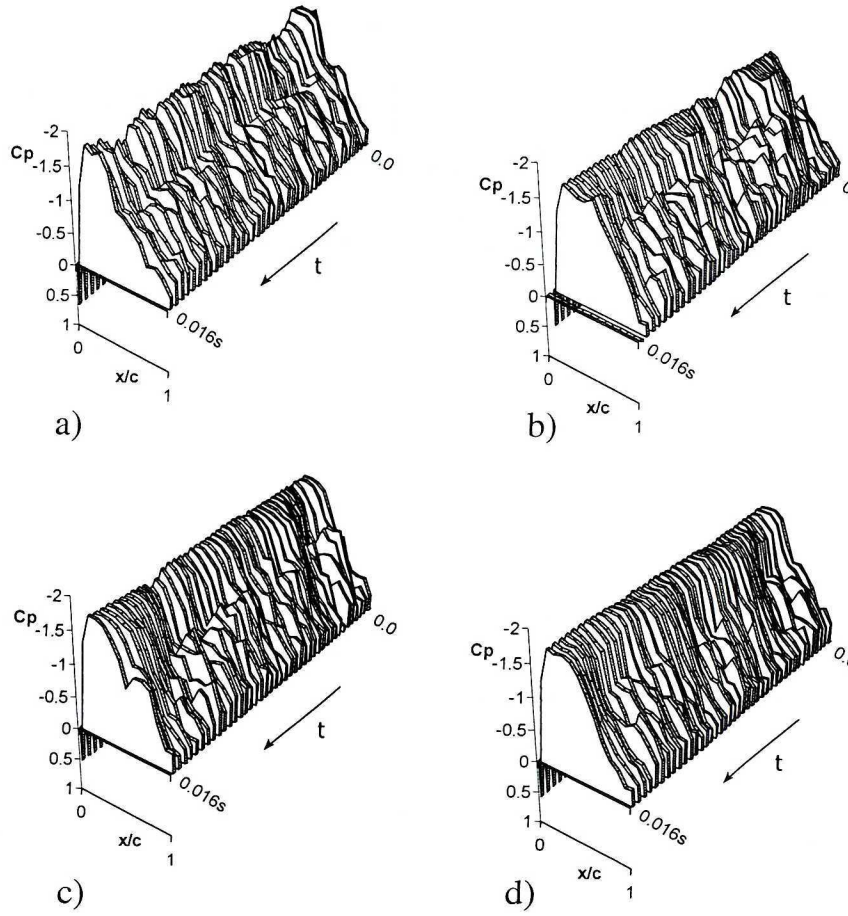

Fig. 10. Momentary pressure distribution on the airfoil upper surface. Free-stream Mach number $M_\infty = 0.7$. Airfoil angle of attack $\alpha = 10°$. Values of initial relative air humidity φ are: a) 12%, b) 40%, c) 60%, d) 80%.

The results are presented in Fig. 11 for various humidity levels ($\varphi = 12\%$, 40%, 60% and 80%) and three characteristic values of angle of attack: $\alpha = 6°$, $\alpha = 8°$ and $\alpha = 10°$.

As it can be seen from Fig. 11a, at $\alpha = 6°$ the pulsations of C_n are very small. No influence of the humidity level of air can be notice.

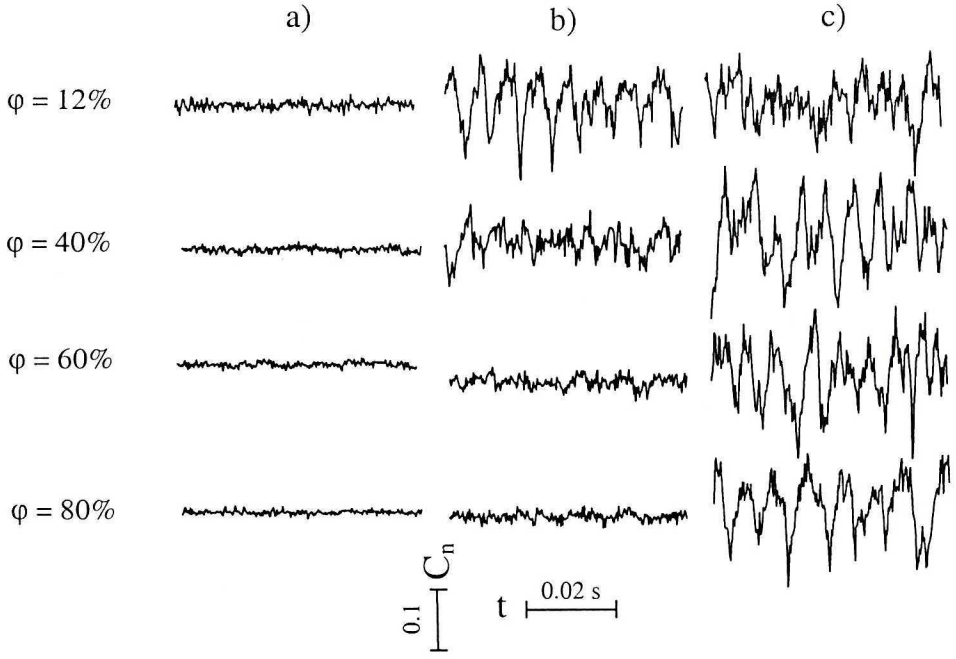

Fig. 11. Time histories of normal aerodynamic force coefficient C_n (component for upper surface only) at $M_\infty = 0.7$. Values of angle of attack α are: a) $\alpha = 6°$, b) $\alpha = 8°$, c) $\alpha = 10°$. Time and pressure scales are the same for all traces.

A different situation can be observed when the buffet occurs. At $\alpha = 8°$ the strongest oscillation of C_n was obtained for humidity level $\varphi = 12\%$. For $\varphi = 40\%$ oscillations of C_n are lower, whereas for $\varphi = 60\%$ and $\varphi = 80\%$ they are not distinguishable. At angle of attack of $\alpha = 10°$ the oscillations of C_n for $\varphi = 12\%$ are lower than those for higher air humidity. This indicates a stronger buffet phenomenon for increased air humidity.

Fig. 12 presents a detailed comparison of all obtained results, where RMS values of the C_n pulsations for various air humidity under consideration are plotted versus angle of attack (with a step of $\Delta\alpha = 0.5°$). For better comparison, all RMS values were normalised using time averaged C_n values at an adequate angle of attack. Owing to this figure, an influence of the humidity level of air on the buffet becomes visible. When the buffet phenomenon does not occur, the C_n pulsation (RMS values) are of order 0.005. When the oscillation of the shock and separation point appears, the RMS value rapidly grows (the value of $dC_n/d\alpha$ is ≈ 0.016).

The higher humidity level of air delays the beginning of the buffet, as it is visible in Fig. 12. At the same time, RMS values of C_n pulsations can take

higher values for humid than for dry air. For humid air, the oscillations of C_n still occur at $\alpha = 10°$.

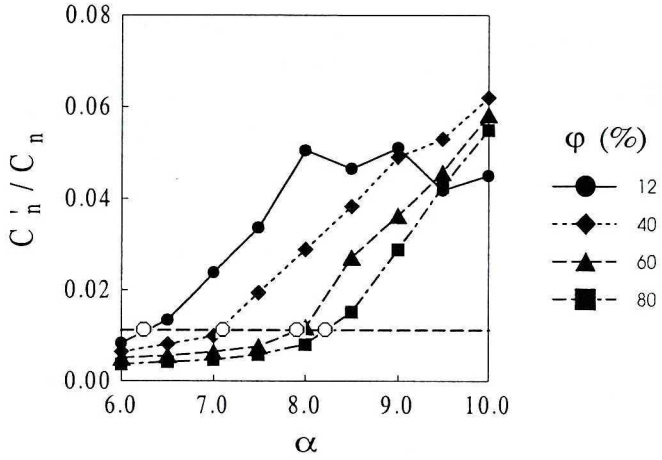

Fig. 12. Normalised RMS values of the C_n pulsation (upper surface component only) versus airfoil angle of attack.

Similar influence of the humidity level of air is presented in Fig. 13, where values of aerodynamic centre of pressure t_p/c are plotted versus the angle of attack α.

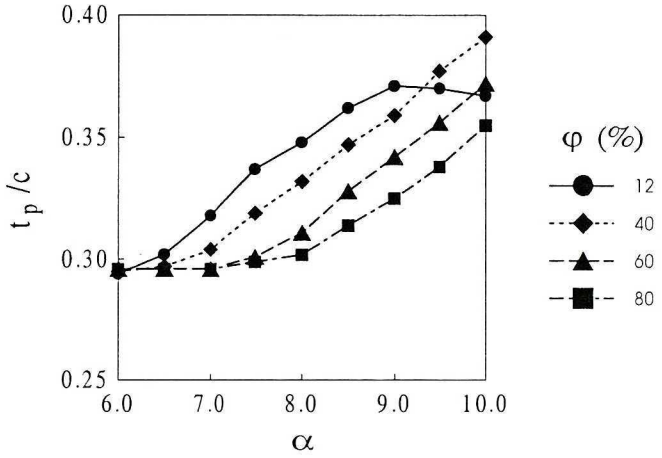

Fig. 13. Normalised values of pressure centre versus airfoil angle of attack.

3.4. Buffet boundary

To determinate the origin of the buffet phenomenon, an explicit criterion should be first defined. The simple criterion in the form of RMS pressure

pulsation value at characteristic airfoil location seems to be insufficient. Thereby, the authors decided to take into account normalised values of normal aerodynamic force pulsation. As the origin of the buffet phenomenon, we assumed the value $C_n'/C_n = 0.1$ (dashed line in Fig. 12) what makes it possible to obtain a separate value of angle of attack for each air humidity level (open circles). A final plot is presented in Fig. 14. As it can be seen from this figure, the humidity of the inflow air delays nearly linearly the origin of the buffet phenomenon.

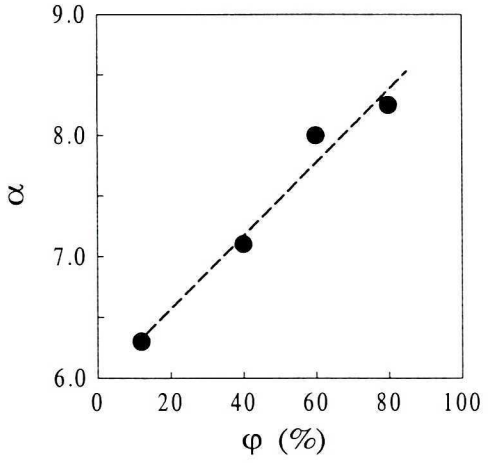

Fig. 14. Airfoil angle of attack characteristic for buffet origin versus air humidity level.

4. Concluding remarks

The humidity level of air has a significant influence on the transonic airfoil flow, especially at higher angles of attack. An increase of the air humidity leads to flow stabilisation, which is associated with decreasing of pressure pulsations. This is due to the changes in average pressure distributions on airfoil surfaces, mainly on the top one. As a consequence, the normal aerodynamic force coefficient as well as the position of the pressure centre are modified.

On the basis of performed experiments it was furthermore found that, the origin of the self-excited oscillations (buffet boundary), shifts to higher angles of attack with increasing of the air humidity level, which is indicated by the variations of the shock as well the separation point position.

This work has been supported by State Committee for Scientific Research in Poland (Project No 7 T07A 026 16).

REFERENCES

[1] Mabey D. G.: Same aspects of aircraft dynamic loads due to flow separation. Progress in Aerospace Sciences, Vol. 26, No. 2, pp. 115÷152, 1989.
[2] Nelson R. C., Pelletier A.: The unsteady aerodynamics of slender wing and aircraft undergoing large amplitude maneuvers. Progress in Aerospace Sciences, Vol. 39, No. 2-3, pp. 185÷248, 2003.
[3] Bean D. E., Wood. N. J.: Experimental investigation of twin-fin buffeting and suppression. Journal of Aircraft, Vol. 33, No. 4, pp. 761÷767, 1996.
[4] Lee B. H. K.: Vertical tail buffeting of fighter aircraft. Progress in Aerospace Sciences, Vol. 36, No. 3-4, pp. 193÷280, 2000.
[5] Lee B. H. K.: Self-sustained shock oscillations on airfoils at transonic speeds. Progress in Aerospace Sciences, Vol. 37, No. 2, pp. 147÷196, 2001.
[6] Flynn G. A., Morrison J. F.: Buffet alleviation on swept and unswept wings at high Incidence. Journal of Aircraft, Vol. 38, No. 2, pp. 368÷377, 2001.
[7] Stanewsky E.: Adaptive wing and flow control technology. Progress in Aerospace Sciences, Vol. 37, No. 7, pp. 583÷667, 2001.
[8] Dor J. B, Mignosi A.: Wind tunnel studies of natural shock wave-separation instabilities for transonic airfoil tests. IUTAM Symposium Transonicum III, DFVLR-AVA Göttingen, 1988, pp. 1÷10.
[9] Nixon D.: Unsteady transonic aerodynamics. Progress in Astronautics and Aeronautics, Vol. 120, 1989.
[10] Swoboda M., Nitsche W.: Shock boundary-layer interaction on transonic airfoils for laminar and turbulent flow. Journal of Aircraft, Vol. 33, No. 1, pp. 100÷1108, 1996.
[11] Schnerr G. H., Dohrmann U.: Transonic flow around airfoils with relaxation and energy supply by homogeneous condensation. AIAA Journal, Vol. 28, No. 7, pp. 1187÷1193, 1990.
[12] Schnerr G. H.: Transonic aerodynamics including strong effects from heat addition. Computer Fluids, Vol. 22, No. 2/3, pp. 103÷116, 1993.
[13] Nosal Z., Selerowicz W.: Transonic airfoil flow of humid air. Cieplne Maszyny Przepływowe – Turbomachinery, No. 117, Vol. 1, pp. 85÷90, 2000 (*in polish*).
[14] Mabey D. G.: A review of scale effects in unsteady aerodynamics. Progress in Aerospace Sciences, Vol. 28, No. 4, pp. 273÷322, 1991.

Manuscript received by Editorial Board, June 04, 2003;
final version, August 21, 2003

Wpływ wilgotności powietrza na zjawisko buffetu

Streszczenie

W pracy badano na drodze eksperymentalnej wpływ wilgotności powietrza na transoniczny opływ profilu NACA0012 w warunkach przepływu, charakterystycznych dla zjawiska buffetu. Rozpatrywano kąty natarcia profilu w zakresie od 6° do 10° oraz poziomy względnej wilgotności powietrza 12%, 40%, 60% i 80%. Na podstawie pomiarów ciśnienia na powierzchni profilu przy różnych poziomach wilgotności, pokazano zmienne w czasie obciążenia profilu, zmianę w czasie składowej normalnej współczynnika siły aerodynamicznej jak również pulsacje siły aerodynamicznej w funkcji kąta natarcia. Zaprezentowano wpływ wilgotności powietrza na początek zjawiska buffetu.